Microstructure and shear strength evolution of a lime-treated clay for use in road construction

Journal:	*International Journal of Pavement Engineering*
Manuscript ID	GPAV-2018-0197.R1
Manuscript Type:	Original Article
Keywords:	lime-treated soils, soil stabilization, clays, microstructural characterization, laboratory tests, shear strength

Note: The following files were submitted by the author for peer review, but cannot be converted to PDF. You must view these files (e.g. movies) online.

Fig.12.jpg

Microstructure and shear strength evolution of a lime-treated clay for use in road construction

The results of a comprehensive experimental programme are presented with the aim of assessing the long-term microstructural modifications as well as evaluating the effects of microstructural rearrangement on the stress-strain behaviour of a lime-treated high-plasticity clay used for road embankments. The stress-strain behaviour at different lime content and curing time was investigated by means of direct shear tests and, simultaneously, microstructural analyses were carried out combining Scanning Electron Microscope observations and Mercury Intrusion Porosimetry tests. The collected results show that the stress-strain behavior of lime-treated clay is strongly dilatant and characterized by a high peak of strength, which increases with time and lime content. Furthermore, a hyperbolic function may be used with the aim to predict the increase in strength at the end of the stabilization process. Microstructural analysis shows that the treatment induces a redistribution of the porosity between macro- and micropores as well as a significant increase of matric suction, measured by means of the filter paper technique. This is also associated to a low reduction of water content and, in clay treated with 2% of lime, to aggregates shrinkage. This peculiar behaviour is affected by lime content and curing time since it results from the formation of the pozzolanic compounds, which mainly develops on the surface of clay aggregates. So, the formation of pozzolanic compounds induces both a bonding between hardened clay aggregates and an increase of their interlocking degree, which is considered as a further contribution to the increase of the shear strength.

Keywords: lime-treated soils; soil stabilization; clays; microstructural characterization; laboratory tests; shear strength

Introduction

Stabilization is a technique commonly used to improve the mechanical behaviour of soils (Bell, 1996; Boardman et al, 2001) and solid waste materials (e.g. biosolids) (Suthagaran et al., 2009; Disfani et al., 2015), that otherwise would not be suitable for earthworks. Several of stabilizers (geogrid, geofiber, lime, cement and many others) can be used as soil additives to improve its engineering properties. The effects of the chemical stabilizers depend on their chemical reactions with the soil elements in presence of water. In the last years, by-products or waste materials from industrial plants were also considered for stabilization in road subgrades or base application. Fly Ash (FA), cement kiln dust (CKD), lime kiln dust (LKD), blast furnace slag and others additives were successfully studied (Al-Rawas et al., 2002; Kang et al., 2015; Puppala, 2016; Mosa et al., 2017). However, experimental research in geotechnical laboratories and in the field has considerably increased the use of lime-based treatments, due to technical, economic and environmental advantages in road construction (Liu et al., 2012; Jawad et al., 2014; Celauro et al., 2015).

Previous studies have dealt with the time-dependent increasing strength of treated soils and nowadays the physic-chemical processes (cation exchange, pozzolanic reactions, etc.) induced by treatment between chemical stabilizers and soils, clay in particular, are well known (Abdi and Wild, 1993; Locat et al., 1990; Metelková et al., 2012; Pomakhina et al., 2012; Zhao et al., 2016; Ho et al., 2017; Choobbasti and Kutanaei, 2017). Moreover, some other studies have focused on the effect on the microstructure of the lime-treated clays (Cuisinier et al., 2011; Russo et al., 2007; Stoltz et al., 2012), also in the long time period (Choquette et al., 1987; Lemaire et al., 2013), as well as on the correlation between microstructural modifications and the improved geotechnical behaviour, e.g. increase of unconfined compression strength, reduction of compressibility and permeability (Al-Mukhtar et al., 2012; Consoli et al., 2012; Di Sante et al., 2014; Wang et al., 2015; Vitale et al., 2017). Furthermore, in-depth analyses were carried out in order to investigate the durability and the microstructural modifications of lime-treated clay when exposed to severe environmental conditions, as water infiltration (Chakraborty and Nair, 2018) or repeated wetting and drying cycles (Tang et al., 2011; Stoltz et al., 2014; Deneele et al., 2016; Rosone et al., 2016b; Rosone et al., 2017).

Very few studies (Mavroulidou et al., 2012; Zhang et al., 2014; Rosone et al., 2018a) have focused so far on the effects of lime treatment on the drained shear strength behaviour. In this connection, a comprehensive analysis of the mechanical behaviour of a complex material, such as a lime-treated clay, should necessarily take into account the dependence on both the microstructural features and their evolution during curing time.

In order to investigate the effect of microstructural rearrangement and the cementation bonding related on the increase of shear strength induced by lime treatment, this paper presents the results of a wide test programme based on an analysis carried out by means of different techniques applied on high-plasticity clay samples treated in a laboratory with different lime contents. The tested materials come from excavation works of an artificial tunnel for a road infrastructure in Sicily (Italy) and have been preliminary tested, according to EN 13286-47 (2004) and 14227-11 (2006), to evaluate the lime affinity for stabilization in road embankments construction. After this evaluation, the mechanical properties have been thoroughly studied by means of direct shear tests carried out on samples saturated by water submersion during the consolidation stage. Simultaneously, a microstructural analysis was performed in order to assess the physico-chemical modifications and the cementitious reactions with time; for this latter purpose the curing period was extended to one year from treatment. Matric suction measurements were also carried out via filter paper method, in order to clarify some macroscopic experimental evidences of the microstructural modifications induced by the lime treatment during the curing time.

Thus, in this paper, the main aim was to combine the test results at different scales in order to relate the comprehensive assessment of both micro- and macro- modifications with the stress-strain behaviour of a lime-treated high-plasticity clay. This approach may provide a significant microstructural perspective of the features induced by lime treatment and how these peculiarities influence the macroscopic behaviour.

Materials and experimental methods

The tested materials come from excavation works of an artificial tunnel for a road infrastructure in Sicily (Airò Farulla et al., 2014). The main geotechnical characteristics and chemical properties of representative samples of the excavation sites are summarized in Table 1.

[Table 1 near here]

An *XRD* diffractometric analysis carried out on the raw material showed the presence of smectite, illite and kaolin and non-clay minerals such as quartz, calcite, feldspar and dolomite. The main characteristics of the quicklime used for the treatment are reported in Table 2.

[Table 2 near here]

The initial consumption of lime (*ICL*), as obtained from laboratory tests (Hilt and Davidson, 1960; Eades and Grim, 1966), was fixed at 1.5%. Preliminary studies were carried out with the aim to define the mix design of the lime-clay mixtures, by means of the evaluation of compaction properties and mechanical performances, in relation to the use for road embankments (Celauro et al., 2012; EN 13286-47, 2004; 14227-11, 2006). Three lime contents were selected (2%, 3% and 4%) in order to be representative of those typically adopted for subgrade and layers of the upper and lower parts of embankments. The results of the mix design tests for the different considered lime contents are summarized in Table 3, in terms of optimum water content, w_{opt}, and maximum dry unit weight, $\gamma_{d,opt}$, for Standard Proctor compaction effort, Immediate Bearing Index, *IBI*, California Bearing Ratio after 4 days of soaking, *CBR(4i)* Index, linear - $\Delta H/H_0$ (ΔH is the variation in height and H_0 is the initial height of sample) - and accelerated volumetric swelling, *Gv*.

[Table 3 near here]

As reported in Table 3, the designed mixtures may be used for the different parts of the embankment since the mechanical performances are higher than the minimum requirements (*CBR(4i)* > *IBI*; *IBI* > 10.5 for the upper part and *IBI* > 8.0 for the lower part of embankment) but they should not be used in layers immediately below the pavement due to their result in terms of volumetric swelling, *Gv*, higher than 5%.

After this preliminary mechanical characterization, in-depth mechanical and microstructural analysis were carried out investigating a wider range of lime content with the aim to better understand the peculiar modifications induced by the treatment, as well as to widen its range of application, independently from a technical evaluation. However, lime contents higher than 6% were not considered due to economic sustainability criteria. So, as-compacted specimens were prepared in laboratory by moistening the selected air-dried material passing through a no. 4 ASTM sieve (mesh opening 4.76 mm), by treating with lime at different lime contents (0, 2, 4 and 6% by dry weight of soil) and statically compacting at the target water content, set equal to the optimum condition under Proctor Standard compaction effort (Table 3). The mixtures were left for 1 hour in an airtight container before compaction for allowing the development of immediate reactions between the quicklime and the soil particles. After compaction, the samples were coated with a transparent plastic film and cured in a climatic chamber with temperature and relative humidity control (T = 20°C,

$RH \geq 90\%$). For the purpose of microstructural analysis, the grain-size distribution curve had to be reduced (maximum apparent particle size equal to 2 mm) (Rosone et al., 2016a) and a small cylindrical mould with a diameter of about 9 mm and a height of 9.3 mm was used.

Suction measurements were carried out by means of Whatman n. 42 filter papers placed in contact with the base of the specimens, in accordance with ASTM D5298 (ASTM, 2016). The soil samples were wrapped in multiple layers of a transparent plastic film and stored in an insulated box for the whole curing period. Matric suction was estimated by means of the water content of the filter papers, according to the calibration formula by Chandler and Gutierrez (1986).

Direct shear tests were carried out on specimens saturated in the shear box at vertical effective stress $\sigma_v' = 100$ kPa and sheared with a horizontal displacement rate equal to 0.002 mm/min. For the samples used in the direct shear tests, the curing time did not include the duration of consolidation (24 h) as well as the duration of the shearing stage (48-60 hours).

Curing times, t, were chosen in accordance with previous experimental evidence (Croft, 1968; Estéoule and Perret, 1979; Boardman et al., 2001) indicating that the stabilization process evolves with time quite quickly at the initial stage and then at a reduced velocity with increasing curing time. Thus, at the beginning, the testing time was set equal to 0, 7, and 14 days and progressively increased to 1, 2, and 6 months. The curing time was later extended up to one year in order to assess the microstructural variation at the end of the cementitious reaction process.

Microstructural analyses were carried out combining Mercury Intrusion Porosimetry (*MIP*) tests and Scanning Electronic Microscope (*SEM*) observations. *MIP* tests were performed using a porosimeter with a maximum intrusion pressure of 200 MPa (corresponding entrance pore diameter of approximately 0.007 μm). The advancing non-wetting contact angle between mercury and the clay minerals was assumed to be 140°

(Romero and Simms, 2008). *SEM* and *MIP* analyses were performed on freeze-dried samples (Delage and Pellerin, 1984). *SEM* observations were performed on gold-palladium coated samples for improving conductivity. This essential treatment represents a limit for adopted experimental technique because every analysis must be carried out on different samples. Anyway, very important morphological information and microstructural changes in the soils can be deduced from comparison of microphotograph (Mandaglio et al., 2016; Rosone et al., 2018c). Analyses were conducted on untreated samples as well as on samples treated with 2, 4 and 6% of lime immediately after treatment (curing time t = 0), after 1 month and after 1 year.

Results analysis

Shear strength behaviour

Fig.1 depicts the shear stress-horizontal displacement (τ-δ_h) curves of the direct shear tests carried out at vertical effective stress σ_v' = 100 kPa. The figure shows that as an effect of short-term reactions in the treated clay, irrespective of the lime content, the peak shear strength τ_p instantaneously increases to a value (τ_p = 139÷151 kPa) equal to about twice the shear strength of the untreated material (τ_p = 73 kPa). The curves for the vertical displacement, δ_v, versus the horizontal displacement, δ_h, are also shown in Fig. 1; positive values of vertical displacement represent dilation of the specimen. As seen in the figures, the behaviour, after treatment, becomes strongly dilatant and characterized by high peaks of strength, which increase in intensity with the curing time and the lime content. However, the horizontal displacement at failure always increases during the overall curing time within the range δ_h = 0.3÷1.5 mm. As expected, the maximum rate of dilation corresponded to the peak strength. Furthermore, the ultimate strength was not fully reached since in some tests the dilation was still ongoing even at a horizontal displacement as large as 6 mm.

Fig. 2a shows the evolution with the curing time of the peak shear strength of clay treated with different lime contents. The material treated with 2% of lime after 14÷28 days reached an almost steady resistance (τ_p = 199 kPa), probably because all the available lime was already consumed and pozzolanic reactions stopped; for lime content equal to 4%, the time required to complete the stabilization process increased to at least 60 days. Conversely, when the clay is treated with 6% of lime, an increase in strength, significantly more evident in the first 60 days, is observed for the whole curing time (180 days). Then the maximum drained shear strength (τ_p = 253 kPa) was measured on the clay treated with 6% of lime after 180 curing days.

The experimental data were interpolated with very good accuracy by means of a hyperbolic function (Gens, 1993; Airò Farulla & Rosone, 2014) modified for predicting the increase in strength with time, as follows:

$$\tau_p = \tau_{p,0} + \frac{t}{\dfrac{1}{r} + \dfrac{t}{\Delta\tau_{p,lt}}} \tag{1}$$

where t is the curing time in days, while $\tau_{p,0}$, r and $\Delta\tau_{p,lt}$ are material parameters. In particular, $\tau_{p,0}$ is the peak shear strength at t = 0, r represents the initial tangent at t = 0 (the initial time evolution of strength) and $\Delta\tau_{p,lt}$ is the long-term increase in strength. The coefficient of determination, R^2, for the different lime contents, varied in the range between 0.928 and 0.994. In Fig. 3 the parameters of the increasing strength equation are reported as a function of the lime content. It is quite evident that, in the range considered, the immediate and long-term increase in strength, ($\tau_{p,0}$ and $\Delta\tau_{p,lt}$) directly depends on the lime content while the time evolution (r), i.e. the rate of strength increase, is essentially independent of lime content.

In Fig. 2b shows that the dilatancy angle at failure ($\nu'_f = \Delta\delta_v / \Delta\delta_h$) of the clay treated with 4% and 6% of lime, also increases as a hyperbolic function of time. The maximum value of the dilatancy angle was approximately 30°, similar to very dense silica sands (Valore et al., 2017; Ziccarelli et al.; 2017) or quartz locked sands (Celauro et al., 2014). The clay treated with 2% of lime initially shows similar behaviour to the one of the samples treated with greater amounts of lime; after 14 days, the dilatancy angle, from a maximum of about 16°, decreases and, for curing times higher than 60 days, reaches a steady value equal to 12°. Therefore, the experimental results show that dilatancy provides a strong component of shear strength in lime-treated soils.

With the aim of depicting failure envelopes of drained strength, experimental data of direct shear tests carried out at vertical effective stress $\sigma_v' = 100 \div 300$ kPa on treated samples after 28 day of curing and untreated clay are reported in Fig. 4. Comparison between the envelopes highlights the effectiveness of lime treatment in a wider range of effective stress, since the envelope of untreated clay is characterized by $c' = 38$ kPa and $\varphi' = 20°$. The obtained peak shear strength parameters are similar to those of other natural high plasticity clays (Cotecchia et al., 2007; Airò Farulla et al., 2015; Rosone et al., 2018b)

The shear strength envelopes of treated clay lie in a tight range far from untreated clay, considering that the peak shear strength angle is quite constant ($\varphi' = 38 \div 40°$) and the intercept cohesion varies with the lime content ($c' = 75 \div 132$ kPa). However, very low increase of strength is obtained after 28 days passing from 4% ($c' = 121$ kPa) to 6% of lime even if, especially for the higher lime content, the long-term shear strength will further increase up to 6 months of curing time (Fig. 2a).

Microstructural modifications

The *SEM* micrograph of the as-compacted untreated clay (Fig. 5) shows an evident massive close packing structure; aggregates of clay plates are assembled in a dispersed arrangement and are largely in mutual contact. Boundary aggregations often cannot be distinguished and only a few μm-sized voids are visible.

The *SEM* microphotograph shown in Fig. 6a highlights the fact that immediately after treatment the microstructure of clay with 2% of lime is characterized by aggregates smaller than those of the untreated clay. Furthermore, aggregates are characterized by edge-to-face and edge-to-edge flocculated texture. Macropores in the order of 30-50 μm are clearly visible although the aggregates are rather compact considering that micropores are indistinguishable inside them. The effect of treatment is more evident at higher lime content, i.e. for samples treated with 4% (Fig. 6b) and 6% (Fig. 6c). In both cases, a more open structure is clearly visible and several nodules of hydrated lime which have not reacted yet are discernible. In particular, the image of the as-compacted samples of clay treated with 6% of lime content brings out a structure completely obliterated by the lime, which has segmented the aggregates and flocculated smaller single particles (Fig. 6c). The flocculated nature of the structure is more evident with treated clay particle clusters interspersed by large openings. Due to the short-term processes (exothermic hydration process, cation exchange), the aggregated structure is transformed into small lump arrangements. Moreover, the more fragmented structure undoubtedly will facilitate the attack gel cementing on the aggregate edges.

After 1 month of curing (Figs. 6d, e and f), it is clearly evident that the flocculation process has progressed further. At the same time, some pozzolanic compounds are already visible. The microstructure of the clay treated with 2% of lime (Fig. 6d) is characterized by some pozzolanic compounds which develop, together with flocculated smaller single particles, several bridges between clay aggregates of higher dimensions. *SEM* microphotographs of clay treated with 4% (Fig. 6e) and 6% (Fig. 6f) show that clay aggregates, still visible in the images taken immediately after the treatment (Figs. 6b and c), have been divided into much more segmented elements while lime particles which have not reacted are still recognizable due to their negligible self-cementing properties (Solanki and Zaman, 2012). However, after 1 month, in the clay treated with 6% of lime (Fig. 6f), pozzolanic compounds formation is already quite visible and persistent.

A *SEM* microphotograph of the sample treated with 2% and cured for 1 year (Fig. 6g) shows a compact structure characterized by very dense aggregates due to the closing of smaller pores on their surface. This process could be related to the cementing of the pozzolanic reaction products, which evidently appears to be limited to the surface of some aggregates. Conversely, the samples with 4% and 6% of lime after 1 year (Figs. 6h and 6i) show similar rather stable structures from both the chemical and morphological points of view, very differently from the original one (i.e. t = 0, Fig. 2b and 2c). In addition, they are almost entirely covered by white cementation compounds due to the completion of the pozzolanic reactions.

SEM microphotographs at low magnification (100x) of samples treated with 2% and 6% of lime 1 year after treatment (Figs. 7a and b) highlight some peculiar characteristics of enhanced microstructures. Macropores in the order of 15-20 μm and long fissure-like pores having width of 3-10 μm between aggregate contacts are clearly visible in the clay treated with 2% of lime. On the other hand, the microstructure of clay treated with 6% of lime is characterized by aggregates with well-defined physical boundaries and intensely interlocked with one another similarly to what happens in calcareous, quartz and pumice sands subjected to very high stresses (e.g. Valore and Ziccarelli, 2009; Ziccarelli, 2016). This microstructural configuration can contribute to increasing the shear strength.

The results of MIP tests are shown in Figs. 8, 9 and 10 in terms of intruded void ratio $e_i = V_{int} / V_S$ (where V_{int} is the cumulative volume intruded by mercury and V_s is the volume of solid), and of Pore Size Density, ($PSD=\delta e_i/\delta(logd)$), as a function of the intruded equivalent diameter, d (Washburn, 1921; Romero and Simms, 2008). The evolution of the characteristics of the samples in terms of initial void ratio, e_0, intruded void ratio, e_i, and non-intruded void ratio, e_0–e_i , are plotted in Fig 11. In this regard, the volume of pores with dimension smaller than the resolution of the *MIP* apparatus (i.e. the inter-layer porosity and the smallest micropores) was considered as negligible since this porosity is significant mainly for high activity clays (Delage et al., 2006; Seiphoori et al., 2014). This hypothesis seems to be confirmed by the evidence that the ending tangent of the intrusion curves is substantially horizontal. Hence the difference (e_0–e_i) between the measured and overall intruded void ratio is primarily the consequence of the non-detected largest pores filled by mercury before the start of the test (Koliji et al., 2010).

Fig. 8 shows the results of tests carried out on an air-dried intact clay fragment (w = 4.5%) as well as on an untreated clay sample statically compacted at optimum conditions (w_{opt}, $\gamma_{d,opt}$) (see Table 3). The intact clay is characterized by a single-mode pore size distribution (Fig. 8b) with a micropore range having a modal value equal to 0.26 μm. The untreated compacted clay presents a double porosity distribution. The smallest pores are those inside the aggregates, while the macropores are those between the aggregates. Excluding pore diameters smaller than 0.07 μm, (very likely still to be filled with water for the sample air-dried at its hygroscopic water content, $w_h \approx 4\%$), the microporosity is strongly influenced by the increase in water content and it is characterized by a very marked peak corresponding to d = 0.5 μm. Assuming the diameter $D_{m\text{-}M}$ = 2.5μm as a limit between the micropores and macropores, the intruded void ratio in the field of macropores, defined as macroporosity void ratio, e_M, is less than 12 % of the total intruded void ratio and shows a uniform size distribution between 3 and 100 μm.

Effect of the lime content

The effects of the lime content (2 and 6%) is evident in Fig. 8. Tests on clay treated with 4% of lime are not reported in the paper due the similarity of their microstructure to that of the samples treated with 6% lime. The treated clays always keep the typical double porosity distribution. The macropore modal value is substantially coincident, equal to about 30 μm, while the macroporosity intruded void ratio e_M increases with the lime content (Fig. 11). Conversely, both the micropore modal value and the micropores intruded void ratio, e_m, decrease with increasing lime content (Fig. 8). The intruded void ratio of the treated specimens increases with the lime content due to the increase macropores intruded void ratio while, as shown, the intruded volume in the micropore field decreases. This result is consistent with the gradual reduction in the dry unit weight due to the increase in the lime content (see Table 3). It was convenient to differentiate the value of the diameter D_{m-M}.

Indeed, *SEM* microscopy observations at $t = 0$ highlighted fragmentation of clay aggregates and consequent dissolution induced by Ca^{2+} cation exchange. This process produces a reduction of the diffuse double layer and flocculation of clay particles due to the reduction in the repelling force (Bhattacharja et al., 2003). Then, the D_{m-M} value was set equal to 1.5 μm for samples treated with 2% of lime and equal to 0.5 μm for samples treated with 6%.

Effect of the curing time

In order to highlight the effect of the curing time, Figs. 9 and 10 present the results of the *MIP* tests carried out on clay treated with 2% and 6% of lime, for curing times of 0 days, 7 days, one month and one year. So far, the *PSD*, irrespective of lime content and curing time, maintains a markedly bimodal arrangement. Moreover, at a constant curing time, the intruded void ratio increases with the lime content. This result, as seen in Fig. 8, is due to ion exchange and flocculation, which lead to an increased inter-aggregate pore volume (macropores).

Conversely, both the volume and the diameters of the micropores decrease, due to the presence of lime compounds on the surface of the aggregates. Nevertheless, the intruded void ratio of micropores is always higher than that of macropores (Fig. 11). The gradual reduction with time of the intruded volume is associated with formation of stable bonding compounds at the particle contact edges due to the long-term effects induced by lime (Russo and Modoni, 2013). Hence, mercury penetration in the micropores is further reduced by tightening of contacts between aggregates. This process, indeed, is significant when clay is treated at a lime content higher than the amount of lime consumed by short-term reactions (Eades and Grim, 1966; Hilt and Davidson, 1960). At the same time, the clay aggregates shrink, probably due to pore water consumption as a consequence of pozzolanic reactions in the inter-aggregate micropores. This contraction ends up in a reduction of the micropore intruded void ratio and, consequently, in a slight increase in the macropores intruded void ratio, due to the increase in the frequency of pores having equivalent diameters between 3 and 15 μm. Overall, the microstructure becomes denser and more stable. The process is strongly marked in clay treated with 2% of lime because aggregates still retain a clayey nature and, therefore they are more subject to volumetric contraction upon drying. Large expanded macropores at the contact between aggregates, as shown in Fig. 7a, 1 year after treatment, may be the consequence of such volumetric shrinkage. At the same time, the reduction in the macropore modal value is caused by partial pore occlusion through the cementing effect of the compounds. A measure of the constricted porosity, defined as the porosity referring to pores that are only accessible through smaller ones (Delage and Pellerin, 1984), is provided by the value of the intruded void ratio at the end of the mercury pressure reduction phase. The difference between the intruded void ratio at the end of the pressure increase and at the end of the pressure decrease, e_{int}-e_{dec}, gives the interconnected void ratio. As reported in Figure 11, the interconnected void ratio decreases with the curing time. The intruded void ratio curves of the clay treated with 6% of lime (Figs. 10) show that the reduction of porosity is evident in the field of pores with a diameter between 0.04 to 0.4 μm while a slight pore volume increase is observed in the range of diameter between 0.4 and 20 μm only. Hence the inter-aggregate porosity (macropores) becomes partially occluded, and partially interconnected too, due to the ink-bottle effect (Russo and Modoni, 2013).

Effect of the pozzolanic reactions

Indeed, the distribution and frequency of the micropores is also affected by the progress of pozzolanic reactions. The diameter corresponding to the peak of micropores is strongly dependent on both the lime content and the curing time. At constant curing time, it decreases with an increase in lime content and, at constant lime content, it decreases with an increase in the curing time. Figure 10 shows that the micropores intruded void ratio of the clay treated with 6% decreases with time since the larger diameters of the intra-aggregate pores, higher than the modal value, decrease in frequency. Thus, the modal value decreases and the micropore distribution slightly shifts to the left side of the diagram (Fig. 10b). In clay treated with 2% of lime content, this phenomenon is substantially limited to the first month of curing since the micropore distribution after 1 year is considerably shifted towards smaller diameters, as discussed before, due to the effect of volumetric shrinkage on clay aggregates. In this regard, matric suction, s, and water content measurements, w, carried out for curing times equal to 7 and 14 days, and 1, 2, 3 and 6 months, reported in Fig. 12, prove that the treated samples were subjected to processes that significantly increased the matric suction and slightly reduced the water content with time. The consumption of water is more evident in the first part of the curing period, due to development of pozzolanic reactions, while a higher increase in matric suction, at almost constant water content, is observed later. However, the lime treatment-induced drying process is deeply affected by the different lime contents, as well as the curing time. The higher suction variations during the overall curing period considered were observed in clay treated with 2% of lime. Under the assumption that soil pores can be considered as a bundle of cylindrical tubes of various diameter subjected to capillarity mechanism, it is possible to link the matric suction to the equivalent pore diameter, d, by means of Laplace's equation ($s = 4\ T_s \cos\theta / d$). Considering the initial measured suction (at t = 7 days) and the final measured suction (at t = 6 months) in Laplace's equation and assuming a surface tension of water T_s of 0.074 N/m (at 20°C) and a zero contact angle θ, it can be considered that pores having diameters in the range of about 0.7μm and 0.1 μm, which were initially subjected to capillary forces, dried during the whole curing time. Fig. 9b shows that in the curing time between 1 month and 1 year, the microstructure of 2% lime treated clay is markedly affected in the above range of diameters. Considering that the water is a fundamental element for the formation of cementing pozzolanic products, this process should be taken into account when long-term microstructure variations are analysed.

Discussion

The high increasing shear resistance can undoubtedly be related to the formation of the pozzolanic reaction products, which act as bonding and also increase the interlocking degree between aggregates. In fact, primarily, the higher persistent areas with developed pozzolanic products, shown in Fig. 3b, are responsible for the highest peak of strength. The development of chemical reactions is progressive in time and shows, as discussed before, intensive microstructural variation during the curing time. The rate of the chemical reaction, correlated to the r parameter of equation (1), seems to be independent of the amount of lime. In fact, in deep analysis of direct shear tests shows that in the first 14 days the increase of strength proceeds with the same rate for different lime contents. Most of the increasing resistance is obtained with the addition of 2% of lime, but if this limit is exceeded, the long-term performance of the treated clay, identified after 180 days, is directly proportional to the amount of lime, at least for the range explored. In fact, the time required to complete the pozzolanic reaction for clay treated with 4 and 6% (60-180 days) is much higher than that for lime treated with 2% (14-28 days). Hence, the time required to complete the process is a direct function of the lime available in the mixture.

In addition to the failure of the cementing bonds, proportional in strength to the amount of lime added, there is a further high contribution to the peak shear strength increase due to the strong interlocking created between the aggregates. The high dilatant contribution, linked to existing interlocking between aggregates, is time-dependent but it is also deeply affected by the amount of added lime (Fig. 2b). The higher dilatant behaviour develops after 1 year, for lime content equal to 6%, when the physical boundaries of aggregates are quite recognizable although widespread products of pozzolanic reactions have linked them (Figs 6i and 7b). Conversely, the expansion of macropores, after 28-60 days, due to aggregate shrinkage in clay treated with 2% of lime, may be responsible for the reduction of the dilatant behaviour in the long-term performance. However, lime treatment can be considered as effective in the behaviour after the peak (Fig. 1) since bonding effects disappear after failure but the results of physical-chemical modifications persist despite the accumulation of shear deformations (Rosone et al., 2018a).

Conclusions

In line with the main aim of this research, the experimental program carried out in this study provided a significant insight on the microstructural features and on their link with the macroscopic behavior of the lime treated clay. In fact, few studies so far have focused on the coupling between micro and macro effects on both the structure and on the drained shear strength of lime treated clay, which is deeply investigated in the present paper. The results confirm that the shear strength of lime-treated clay is a function of lime content, since it affects the extent of cementing bonds as well as the intensity of the dilatant behaviour. It is possible to conclude that the lime treatment is a markedly time-dependent process that induces not only macroscopic improvements in the mechanical response of the treated soil, but also fundamental microstructural modifications. In particular, the microstructural analysis shows that the treated clay keeps a typical double porosity distribution irrespective of the microstructural variations, which are strongly dependent on the amount of lime and the curing time.

Lime content higher than the quantity of lime consumed by the short-term reactions (ICL) induces a redistribution of the porosity, with a reduction of the micropore volume and an increase in the volume of macropores. In this connection, pozzolanic products are able to partially fill the pores and reduce the microporosity. This process, linked to development of pozzolanic reactions, is time-dependent and is already significant for curing times lower than 1-2 months.

As proved by MIP analysis, long-time pore size distribution, at least for low lime content values, is also affected by volumetric shrinkage of aggregates, due to matric suction and water content variations, and consequently induced variation in macropores. Thus, the development of the improved mechanical behaviour due to lime addition is proved to be closely linked to microstructural features such as the formation of pozzolanic reaction products (bonding) as well as to the increase in the interlocking degree between aggregates. This evidence may be of particular interest when predicting the long-term behaviour as well as the long term resistance of the stabilized soils for design purposes in road construction.

References

Abdi M.R., Wild S., (1993). Sulphate expansion of lime-stabilized kaolinite: I. Physical characteristics. *Clay Minerals*, 28 (4), 555-567.

Airò Farulla C., Celauro B., Celauro C., Rosone M., (2014). Field test of lime treatment of clayey soils for railways and road works. *Ingegneria Ferroviaria,* 69 (9), 729-752.

Airò Farulla C., Cafiso F., Calvi F., Rosone, M. (2015). Safeguarding historic towns on hilltops threatened by land sliding: The case of San Fratello in Sicily. *Italian Geotechnical Journal*, 49 (1), 7-28.

Airò Farulla, C., Rosone, M. (2014) Modeling Round Robin test: an uncoupled approach. *Procedia Earth and Planetary Science*, 9, 195-200.

Al-Mukhtar M., Khattab S., Alcover J.F. (2012). Microstructure and geotechnical properties of lime-treated expansive clayey soil. *Engineering Geology*, 139-140, 17-27.

Al-Rawas A.A., Taha R., Nelson J.D., Al-Shab T.B., Al-Siyabi H. (2002). A comparative evaluation of various additives used in the stabilization of expansive soils. *Geotechnical Testing Journal*, 25(2), 199–209.

ASTM D5298-16 (2016). Standard Test Method for Measurement of Soil Potential (Suction) Using Filter Paper, ASTM International, West Conshohocken, PA, 2016.

Bhattacharja S., Bhatty J.I., Todres H.A., (2003). Stabilization of Clay Soils by Portland Cement or Lime – A Critical Review of Literature. Portland Cement Association, Skokie, Illinois (USA). PCA R&D Serial No. 2066.

Bell F.G., (1996). Lime stabilization of clay minerals and soils. *Engineering Geology,* 42 (4), 223-237.

Boardman D.I., Glendinning S., Rogers C.D.F., (2001). Development of stabilisation and solidification in lime-clay mixes. *Géotechnique.* 51 (6), 533-543.

Celauro B., Bevilacqua A., Lo Bosco D., Celauro C. (2012). Design Procedures for Soil-Lime Stabilization for Road and Railway Embankments. Part 1 - Review of Design Methods. *Procedia - Social and Behavioral Sciences*, 53, 754-763.

Celauro C., Corriere F., Guerrieri M., Casto B.L. (2015). Environmentally appraising different pavement and construction scenarios: A comparative analysis for a typical local road. *Transportation Research Part D: Transport and Environment*, 34:41-51.

Celauro, C., Ziccarelli, M., Parla, G. & Valore, C. (2014) An automated procedure for computing the packing properties of dense and locked sands by image analysis of thin sections. *Granular Matter* 16(6), 867-889.

CEN EN 14227-11 (2006). Hydraulically bound mixtures — Specifications — Part 11: Soil treated by lime. European Standards (EN) CEN European Committee for Standardization, Brussels, Belgium.

CEN EN 13286-47 (2004). Unbound and hydraulically bound mixtures — Part 47: Test method for the determination of the California bearing Ratio, Immediate Bearing Index and linear swelling". European Standards (EN) CEN European Committee for Standardization, Brussels, Belgium.

Chakraborty S., Nair S. (2018). Impact of curing time on moisture induced damage in lime-treated soils. *International Journal of Pavement Engineering*, DOI: 10.1080/10298436.2018.1453068. 1-13.

Chandler R.J., Gutierrez C.I. (1986). The filter paper method for suction measurement. *Géotechnique,* 6 (2), 265-168.

Choobbasti A.J., Kutanaei S.S. (2017). Microstructure characteristc of cement-stabilized sandy soil using nanosilica. *Journal of Rock Mechanics and Geotechnical Engineering*, 9 (5), 981-988.

Choquette M., Bérubé M.A., Locat J. (1987). Mineralogical and microtextural changes associated with lime stabilization of marine clays from eastern Canada. *Applied Clay Science*, 2 (3), 215-232.

Consoli N.C., Johann A.D.R., Gauer E.A., Santos V.R.D., Moretto R.L., Corte M.B. (2012). Key parameters for tensile and compressive strength of silt–lime mixtures. *Géotechnique Letters*, 2 (3), 81-85.

Cotecchia F., Vitone C., Cafaro F., Santaloia F. (2007). The mechanical behaviour of intensely fissured high plasticity clays from Daunia. *Characterisation and Engineering Properties of Natural Soils*, 3, 1975-2001.

Croft J.B. (1968). The structures of soils stabilized with cementitious agents. *Engineering Geology,* 2 (2), 63–80.

Cuisinier O., Auriol J.C., Le Borgne T., Deneele D. (2011). Microstructure and hydraulic conductivity of a compacted lime-treated soil. *Engineering Geology,* 123 (3), 187-193.

Delage P., Marcial D., Cui Y.J., Ruiz X. (2006). Ageing effects in a compacted bentonite: a microstructure approach. *Géotechnique* 56 (5), 291–304.

Delage P., Pellerin F.M. (1984). Influence de la lyophilisation sur la structure d'une argile sensible du Quebec. *Clay Minerals*, 19 (2), 151-160.

Deneele D., Le Runigo B, Cui Y.J., Cuisinier O., Ferber V. (2016). Experimental assessment regarding leaching of lime-treated silt. *Construction and Building Materials*, 112, 1032-1040.

Di Sante M., Fratalocchi E., Mazzieri F., Pasqualini E. (2014). Time of reactions in a lime treated clayey soil and influence of curing conditions on its microstructure and behaviour. *Applied Clay Science*, 99, 100-109.

Eades J., Grim R. (1966). A quick test to determine lime requirements of lime stabilization. *Highway Research Record*, 139, 61-72.

Estéoule J., Perret P. (1979). Etude expérimentale des phénomènes de stabilisation des sols fins par la chaux. *Bulletin de Liaison des Laboratoires des Ponts et Chaussées*, 99, 99-109.

Gens A. (1993). Shear strength. In: *Proceeding of unsaturated soils: recent developments and applications*. Civil Engineering European Courses. UPC Barcelona, Spain, 1-13.

Hilt G., Davidson D. (1960). Lime fixation in clayey soils. *Highway Research Board Bulletin,* 262, 20–32.

Ho L.S., Nakarai K., Ogawa Y., Sasaki T., Morioka M. (2017). Strength development of cement-treated soils: Effects of water content, carbonation, and pozzolanic reaction under drying curing condition. *Highway Research Record*, 134(Supplement C), 703-712.

Jawad I.T., Taha M.R., Majeed Z.H., Khan T.A. (2014). Soil stabilization using lime: Advantages, disadvantages and proposing a potential alternative. *Research Journal of Applied Science Engineering and Technology*, 8 (4), 510-520.

Kang X., Kang G.C., Chang K.T., Ge L. (2015). Chemically Stabilized Soft Clays for Road-Base Construction. *Journal of Materials in Civil Engineering*, 27(7), 04014199.

Koliji A., Vulliet L., Laloui L. (2010). Structural characterization of unsaturated aggregated soil. *Canadian Geotechnical Journal*, 47 (3), 297-311.

Lemaire K., Deneele D., Bonnet S., Legret M. (2013). Effects of lime and cement treatment on the physicochemical, microstructural and mechanical characteristics of a plastic silt. *Engineering Geology*, 166, 255-261.

Liu M.D., Indraratna B., Horpibulsuk S., Suebsuk J. (2012). Variations in strength of lime-treated so clays. Proc. of the Inst. of Civil Eng. 165 (4), 217-223.

Locat J., Berube M.A., Choquette M. (1990). Laboratory investigations on the lime stabilization of sensitive clays: shear strength development. *Canadian Geotechnical Journal*. 27 (3), 294-304.

Mandaglio M.C., Moraci N., Rosone M., Airò Farulla C. (2016). Experimental study of a naturally weathered stiff clay". *Canadian Geotechnical Journal*, 53 (12), 2047-2057.

Mavroulidou M., Zhang X., Gunn M.J., Cabarkapa Z. (2012). An Investigation of the effects of cementation and suction on lime treated London Clay. In: Jotisankasa et al. (eds) *Unsaturated soils 2011: theory and practice*, Papaya, Thailand, Kasetsart University Thailand, pp 527–532.

Metelková Z., Boháč J., Přikryl R., Sedlářová I. (2012). Maturation of loess treated with variable lime admixture: Pore space textural evolution and related phase changes. *Applied Clay Science,* 61, 37-43.

Mosa, A. M., Taher, A. H. & Al-Jaberi, L. A. (2017) Improvement of poor subgrade soils using cement kiln dust. *Case Studies in Construction Materials*, 7:138-143.

Pomakhina E., Deneele D., Gaillot A.C., Paris M., Ouvrard G. (2012). NMR investigation of pozzolanic reaction occurring in lime-treated Ca-bentonite. *Cement and Concrete Research*, 42 (4), 626-632.

Puppala A.J. (2016). Advances in ground modification with chemical additives: from theory to practice. *Transportation Geotechnics*, 9, 123-138.

Romero E., Simms P. (2008). Microstructure investigation in unsaturated soils: a review with special attention to contribution of mercury intrusion porosimetry and environmental scanning electron microscopy. *Geotechnical and Geological Engineering*, 26, 705-727.

Rosone M., Airò Farulla C.,Ferrari A. (2016a). Shear strength of a compacted scaly clay in variable saturation conditions, *Acta Geotechnica*, 11(1), 37-50.

Rosone M., Airò Farulla C., Ferrari A., Torta C., Celauro C. (2016b). Suction controlled drying and wetting cycle effects on the volumetric behaviour of a lime-treated high plasticity clay. *E3S Web of Conference*, 3rd European Conference on Unsaturated Soils – "E-UNSAT 2016", 9, 14020.

Rosone M., Airò Farulla C., Celauro C., Ferrari A. (2017).. Volumetric Behaviour of Lime Treated High Plasticity Clay Subjected to Suction Controlled Drying and Wetting Cycles. In: Ferrari A., Laloui L. (eds) *Advances in Laboratory Testing and Modelling of Soils and Shales (ATMSS), ATMSS 2017*. Springer Series in Geomechanics and Geoengineering. Springer, Cham.

Rosone M., Ferrari A., Celauro C., (2018a). On the hydro-mechanical behaviour of a lime-treated embankment during wetting and drying cycles. *Geomechanics for Energy and the Environment* 14, 48-60.

Rosone M., Ziccarelli M., Ferrari A., Airò Farulla, C. (2018b). On the reactivation of a large landslide induced by rainfall in highly fissured clays. *Engineering Geology*, 235, 20-38.

Rosone M., Ferrari A., Ziccarelli M., Giger (2018c). The residual shear strength of the shaly and sandy facies of the Opalinus Clay. *International Symposium on Energy Geotechnics - SEG 2018*, https://doi.org/10.1007/978-3-319-99670-7_53.

Russo G., Dal Vecchio S., Mascolo G. (2007). Microstructure of a Lime Stabilised Compacted Silt. In *Experimental Unsaturated Soil Mechanics* (Physics, S. P. I. (ed)), vol. 112, pp. 49-56.

Russo G., Modoni G. (2013). Fabric changes induced by lime addition on a compacted alluvial soil. *Geotechnical Letters,* 3 (2), 93-97.

Solanki P., Zaman M. (2012). Microstructural and Mineralogical Characterization of Clay Stabilized Using Calcium-Based Stabilizers. In *Scanning Electron Microscope*. Kazmiruk, V., In-Tech, pp. 771-798.

Seiphoori A., Ferrari A., Laloui L. (2014). Water retention behaviour and microstructural evolution of MX-80 bentonite during wetting and drying cycles. *Géotechnique,* 64 (9), 721-734.

Stoltz G., Cuisinier O., Masrouri F. (2012). Weathering of a lime-treated clayey soil by drying and wetting cycles. *Engineering Geology*, 181, 281-289.

Stoltz G., Masrouri F., Cuisinier O. (2014). Multi-scale analysis of the swelling and shrinkage of a lime-treated expansive clayey soil. *Applied Clay Science,* 61, 44-51.

Suthagaran V., Arulrajah A., Bo M.W., Wilson J. (2009). Stabilisation of biosolids with admixtures for potential use as an embankment fill material. *Australian Geomechanics Journal* 44(3), 63-70.

Tang A.M., Vu M.N., Cui Y.J. (2012) Effects of the maximum soil aggregates size and cyclic wetting-drying on the stiffness of a lime-treated clayey soil. *Géotechnique*, 61 (5), 421-429.

Valore C., Ziccarelli M. (2009). The evolution of grain-size distribution of sands under 1-D compression. *17th International Conference of Soil Mechanics and Geotechnical Eng*ineering, Alexandria, Egypt, October 2009, M. Hamza et al (Eds). IOS Press, 1, 84-88.

Valore, C., Ziccarelli, M., Muscolino, S.R. (2017). The bearing capacity of footings on sand with a weak layer. *Geotechical Research ICE* 4(1), 12-29.

Vitale E., Deneele D., Paris M., Russo G. (2017). Multi-scale analysis and time evolution of pozzolanic activity of lime treated clays. *Applied Clay Science,* 141, 36-45.

Wang Y., Cui Y.J., Tang A.M., Tang C., Benahmed N. (2015). Effects of aggregate size on water retention capacity and microstructure of lime-treated silty soil. *Geotechnical Letters*, 5 (4), 269-274.

Washburn E.W. (1921). The dynamics of capillary flow. *Physical Review*, 17 (3), 273.

Zhang X., Mavroulidou M., Gunn M.J., Sutton J., Cabarkapa Z., Kichou Z. (2014). Application of a novel laser sensor volume measurement system to the triaxial testing of an unsaturated lime-treated soil. *Acta Geotechnica*, 9 (6), 945-957.

Zhao Y., Gao Y., Zhang Y, Wang Y. (2016). Effect of fines on the mechanical properties of composite soil stabilizer-stabilized gravel soil. *Construction and Building Materials*, 126 (6), 701-710.

Ziccarelli M. (2016). Evolution of grain-size distribution of pumice sands in 1-D compression. *Procedia Engineering*, Elsevier, 158C(6), 27-32.

Ziccarelli, M., Valore, C., Muscolino, S.R., Fioravante V. (2017). Centrifuge tests on strip footings on sand with a weak layer. *Geotechnical Research* ICE 4(1), 47-64

List of tables

List of Figures

Figure 10. Time evolution of intruded void ratio (a) and pore size distribution (b) of clay treated with 6% of lime.

Figure 11. Time evolution of void ratio e_0, intruded void ratio at the end of the pressure increase phase, e_{int}, intruded void ratio at the end of the pressure decrease phase, e_{dec}, microporosity void ratio, e_m, and macroporosity void ratio, $e_{M,}$ for clay treated with 2% (a) and 6% (b) of lime.

Figure 12. Matric suction and water content measurements carried out on samples treated with 2, 4 and 6% of lime after 7 and 14 days, 1, 2, 3 and 6 months.

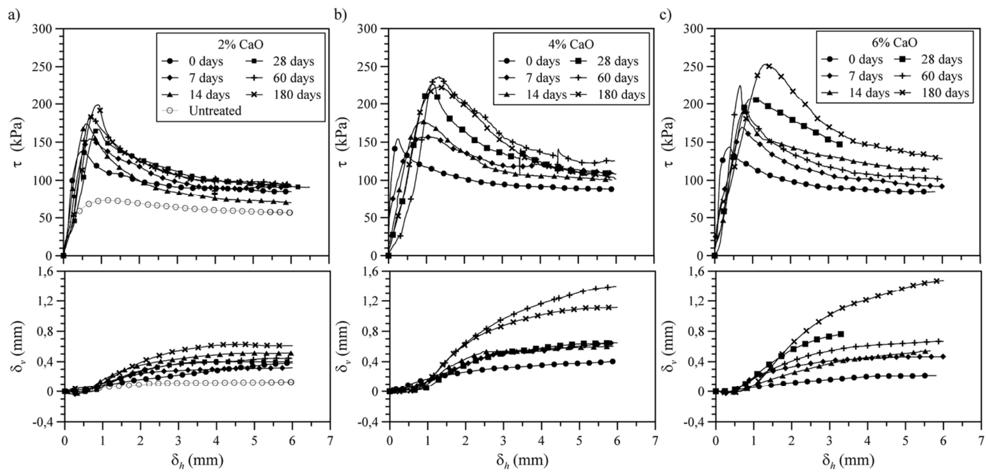

Fig. 1 Shear stress-shear displacement curves and vertical displacement versus horizontal displacement curves from direct shear tests carried out at σ′v = 100 kPa for clay treated with 2% (a), 4% (b) and 6% (c) of lime.

76x36mm (600 x 600 DPI)

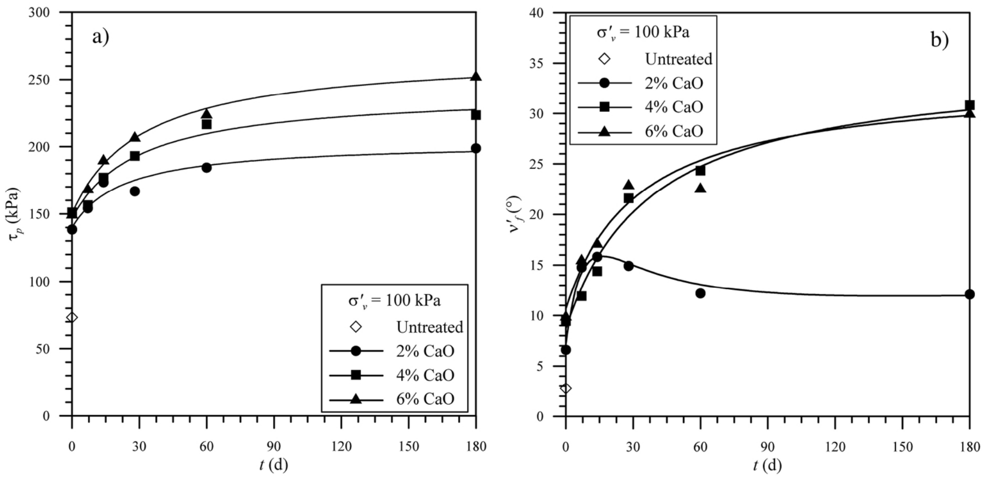

Figure 2. Evolution with the curing time of peak shear strength τp (a) and dilatancy angle at failure v′f (b) at σ′v = 100 kPa for different lime contents.

77x37mm (600 x 600 DPI)

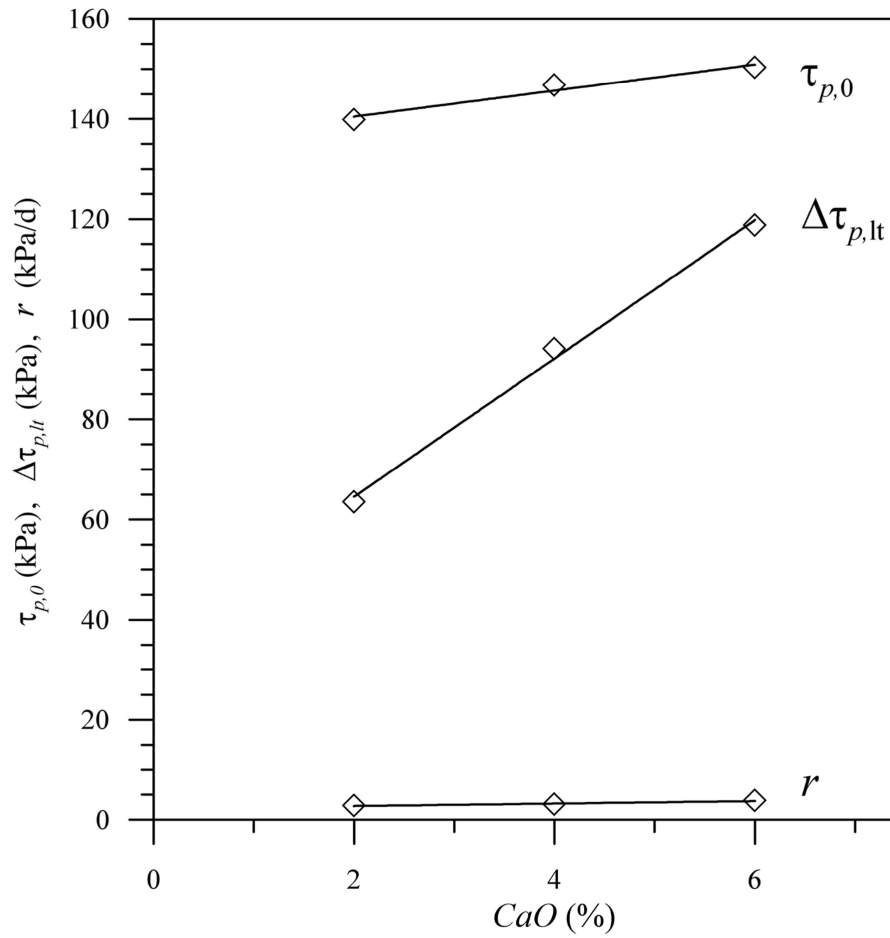

Figure 3. Parameters of increasing shear strength equation for different lime contents of CaO.

77x74mm (600 x 600 DPI)

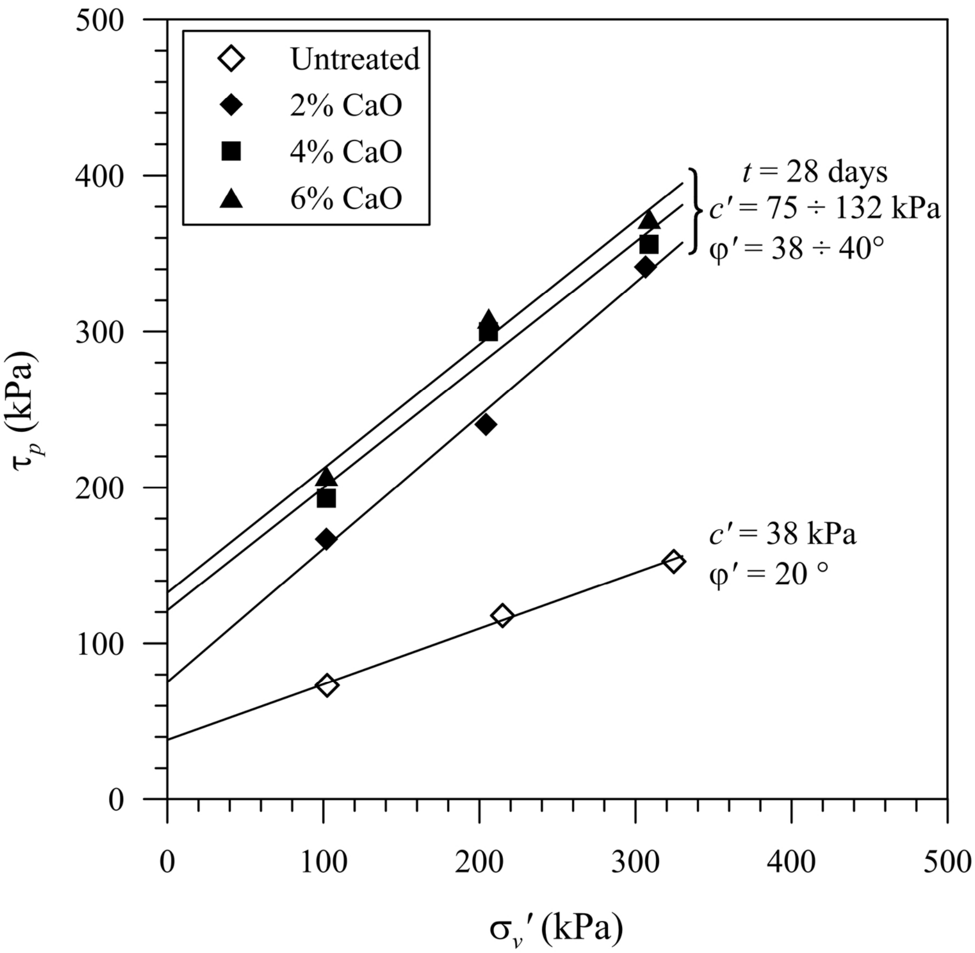

Figure 4. Shear strength envelope for untreated and treated clay after 28 days of curing time.

77x75mm (600 x 600 DPI)

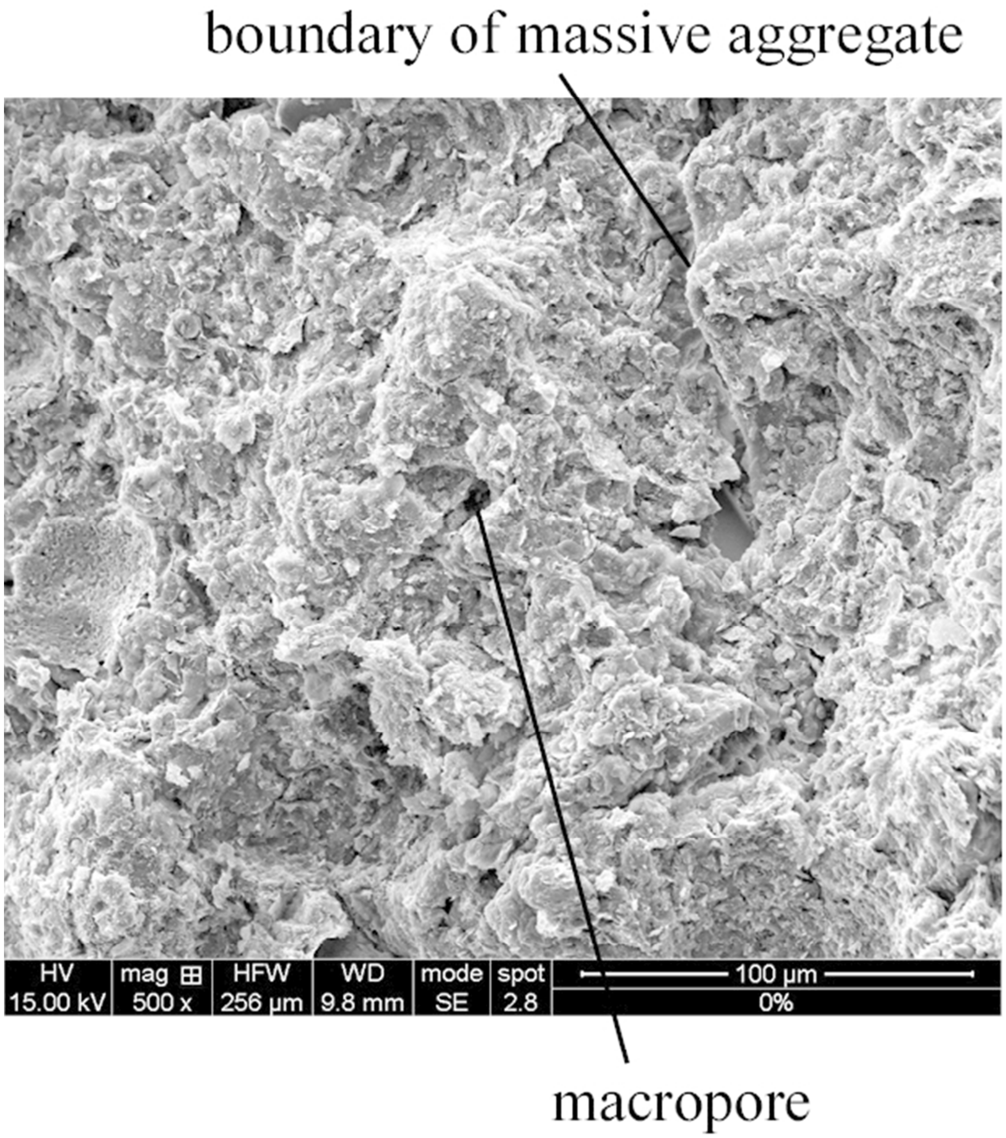

Figure 5. SEM observation of samples of untreated clay.

60x69mm (260 x 260 DPI)

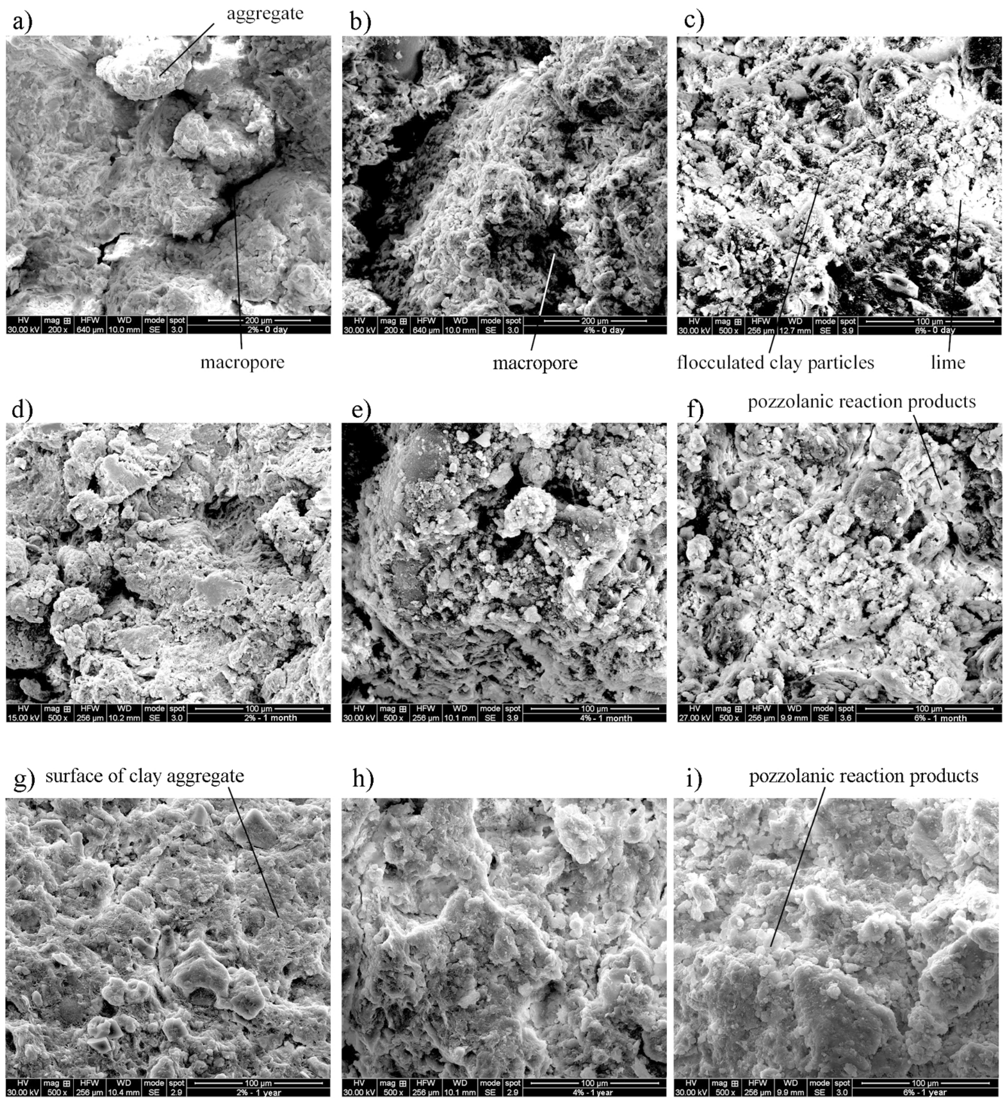

Figure 6. SEM microphotographs of samples of clay treated with 2% (a,d,g), 4% (b,e,h) and 6% (c, f, i) of lime respectively for 0 day, 1 month and 1 year.

160x180mm (300 x 300 DPI)

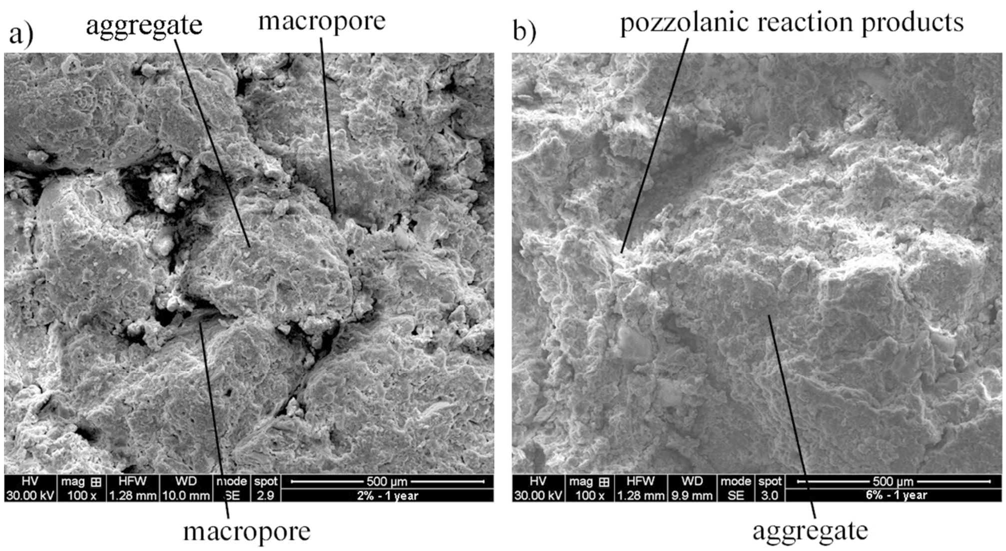

Figure 7. SEM microphotographs at low magnification (100x) of treated clay with 2% (a) and 6% (b) of lime after 1 year of curing.

120x66mm (265 x 265 DPI)

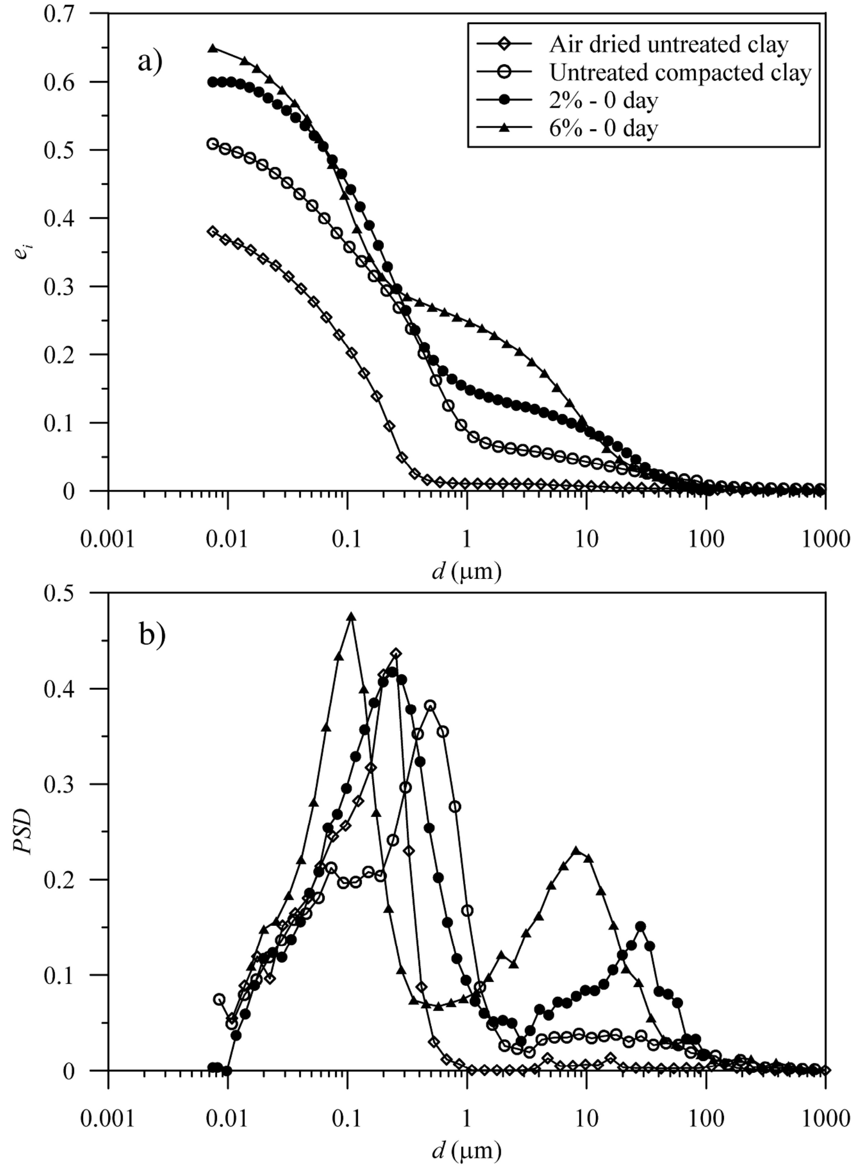

Figure 8. MIP test results carried out after compaction (0 day).

109x151mm (600 x 600 DPI)

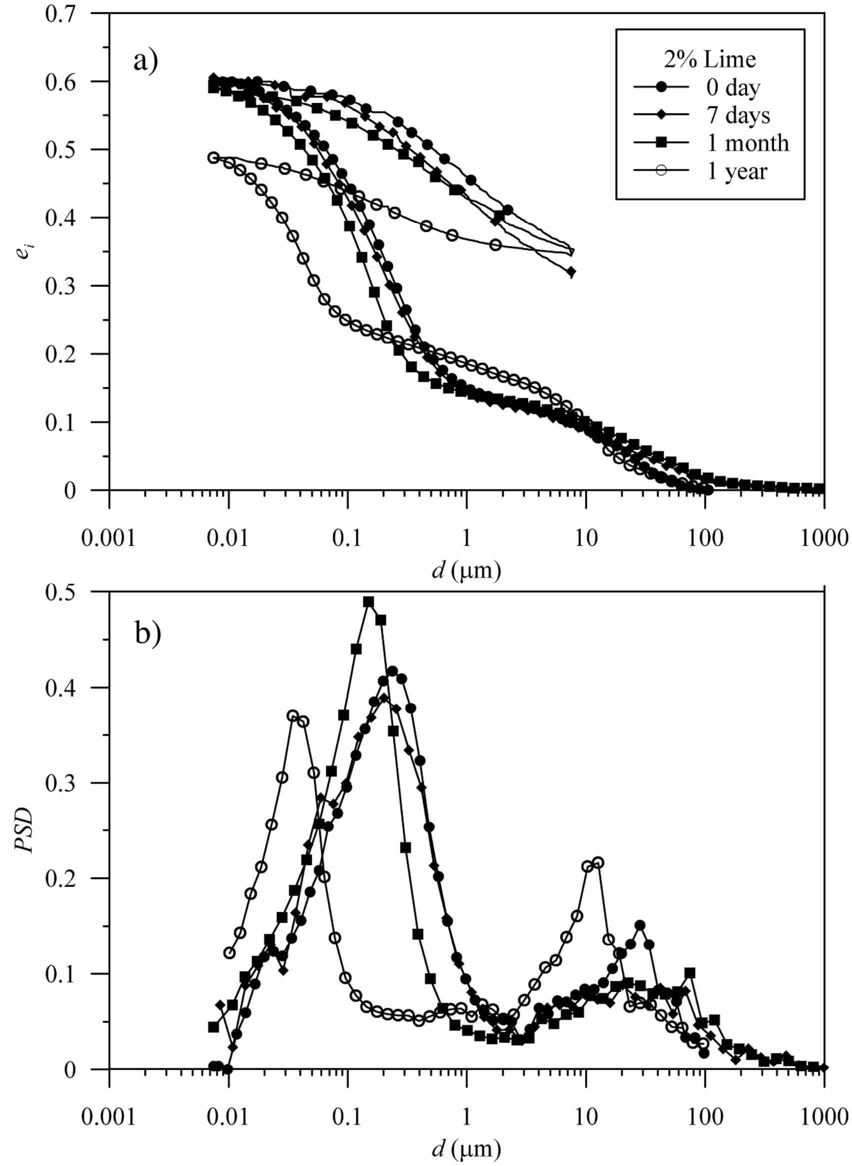

Figure 9. Time evolution of intruded void ratio (a) and pore size distribution (b) of clay treated with 6% of lime.

108x148mm (600 x 600 DPI)

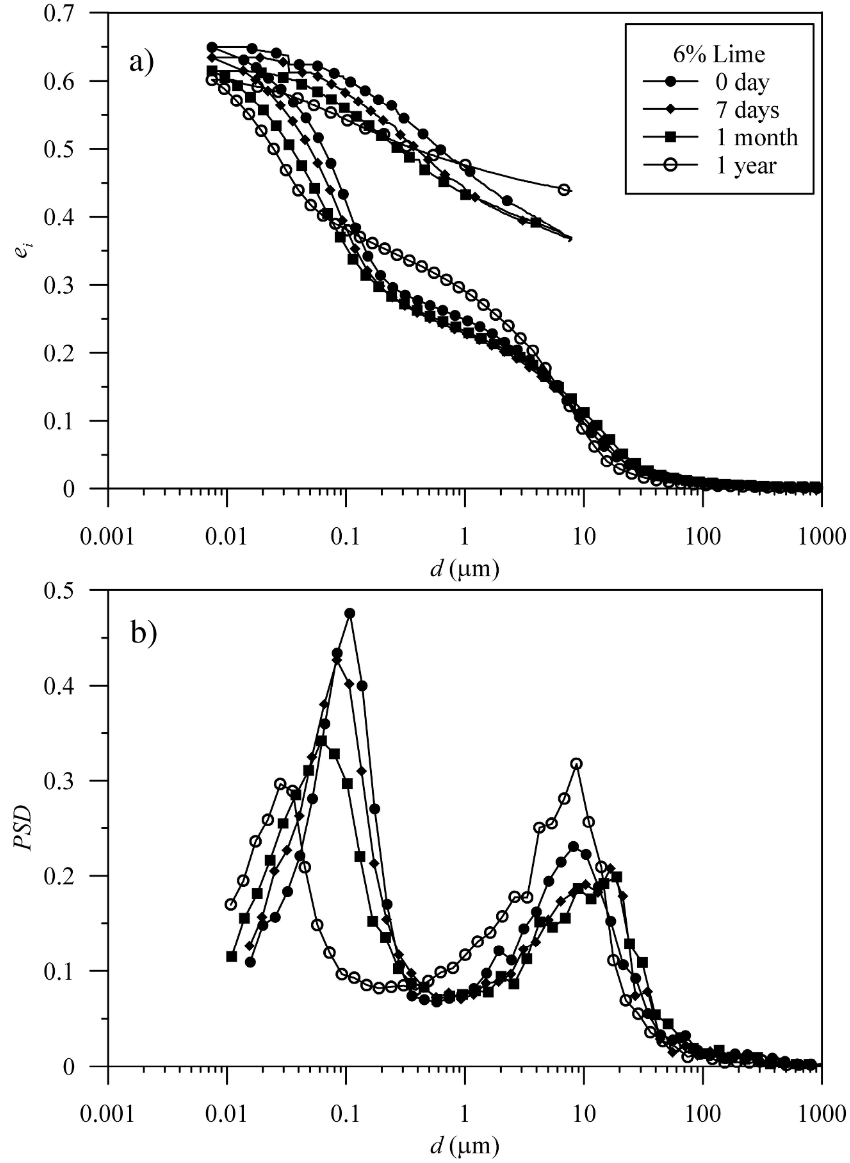

Figure 10. Time evolution of intruded void ratio (a) and pore size distribution (b) of clay treated with 6% of lime.

107x145mm (600 x 600 DPI)

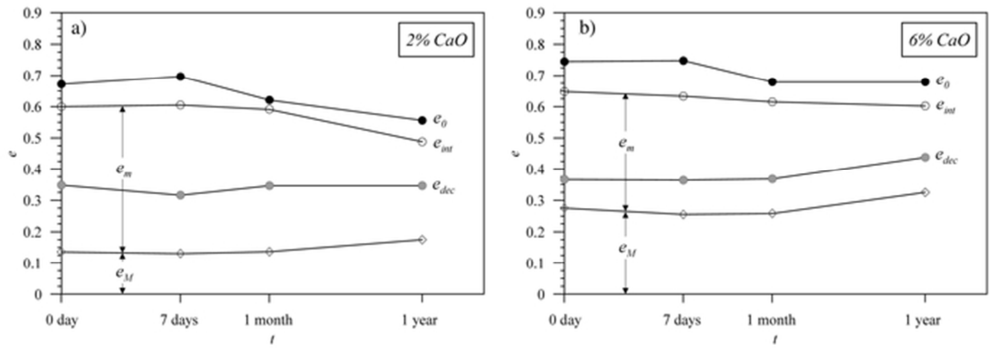

Figure 11. Time evolution of void ratio e0, intruded void ratio at the end of the pressure increase phase, eint, intruded void ratio at the end of the pressure decrease phase, edec, microporosity void ratio, em, and macroporosity void ratio, eM, for clay treated with 2% (a) and 6% (b) of lime.

58x21mm (300 x 300 DPI)

Tables

Table 1. Main geotechnical characteristics and chemical properties of the clay

Water content w_n (%)	Sand fraction f_{sand} (%)	Silt fraction f_{silt} (%)	Clay fraction f_{clay} (%)	Liquid limit w_l (%)	Plastic limit w_p (%)	Plasticity index PI (%)	Activity A	Specific gravity G_S	Sulph. content SO_4 (%)	Org. Matter content S_{OM} (%)	Initial consumption of lime (%)
25.3	6	50	44	53	21	32	0.73	2.69	0.17	2.8	1.5

Table 2. Characteristics of the quicklime

Classification (UNI EN 459-1)	Passing through sieve d = 2 mm (%)	Passing through sieve d = 0.2 mm (%)	Passing through sieve d = 0.075mm (%)	Available lime CaO (%)	Magnesium oxide Content MgO (%)	Water reactivity t_{60} (min)
CL90-Q	100	99.0	81.3	94.5	1.3	3

Table 3. Results of mix design characterization of soil-lime mixtures.

CaO (%)	Optimum water content w_{opt} (%)	Maximum dry unit weight $\gamma_{d,opt}$ (kN/m^3)	Void ratio *e* (-)	Degree of Saturation S_r (%)	Immediate Bearing Index *IBI* (%)	California Bearing ratio *CBR(4i)* (%)	Linear swelling $\Delta H/H_0$ (%)	Volumetric swelling G_V (%)	Use for layers of the embankment
0	20.0	16.1	0.64	84.7	24	-	-	-	Lower part
2	22.0	15.3	0.72	82.0	29	31	1.05	-	Upper part
4	22.4	15.1	0.75	80.5	25	29	1.25	6.9	Upper part
6	22.9	14.8	0.80	80.2	-	-	-	-	-